International Journal of Environmental Sciences
ISSN: 2229-7359
Vol. 11 No. 14s 2025
https://www.theaspd.com/ijes.php

Effect of Tool Geometry and Process Parameters on the Mechanical and Microstructural Properties of AZ31B-SiC Composite

Ravindra Parkhe[1*], Kanif Markad[2], Padmakar Kabudke[3]
[*1]Research scholar, DVVP COE Ahilyanagar, Maharashtra, India
[2]Associate Professor, DVVP COE Ahilyanagar, Maharashtra, India
[3]Assistant Professor, Pravara Rural Engineering College Loni, Maharashtra, India

Abstract
This investigation explores the fabrication of AZ31B magnesium alloy surface composites, enhanced with silicon carbide particulate reinforcement via Friction Stir Processing, and characterizes their mechanical properties. The groove method facilitated the introduction of SiC reinforcement into the AZ31B matrix, a lightweight alloy recognized for its elevated strength-to-weight ratio. A systematic L9 orthogonal array design was implemented to modulate critical processing variables, including tool rotational speed, traverse speed, groove width, and tool pin geometry. Mechanical characterization encompassed tensile strength assessments and Vickers microhardness evaluations, alongside microstructural examination utilizing Optical Microscopy and Scanning Electron Microscopy. The configuration employing a square tool geometry, operated at 545 rpm and a 31.5 mm/min traverse speed, yielded the most refined grain morphology and a homogeneous distribution of SiC particles. This specific processing condition resulted in a peak tensile strength of 152.37 MPa and a hardness value of 100.54 HV. Conversely, elevated traverse speeds and expanded groove widths induced agglomeration of the reinforcement particles, thereby diminishing the mechanical performance of the resulting composites. The results conclusively demonstrate that optimizing FSP parameters is crucial for enhancing the microstructure and mechanical attributes of AZ31B-SiC surface composites, thereby broadening their applicability in diverse structural and lightweight engineering contexts.
Keywords: Friction stir processing (FSP), AZ31B magnesium alloy, SiC reinforcement, mechanical characteristics, microstructural analysis, and optimal parameters.

INTRODUCTION

Magnesium alloys are valued for their unique characteristics, including low density, high specific strength, and excellent machinability, rendering them well-suited for lightweight structural applications in aerospace, automotive, and biomedical sectors. Magnesium alloy AZ31B, composed of aluminum, zinc, and manganese, has garnered substantial interest due to its balanced mechanical properties, corrosion resistance, and ease of fabrication. However, magnesium alloys face certain limitations, such as low hardness, poor wear resistance, and limited creep strength, necessitating the employment of surface modification techniques to enhance their performance in demanding environments.

Magnesium alloys stand out as an exceptional class of materials, offering a significantly lower density compared to aluminium and steel, by approximately 40% and 78%, respectively. This distinctive property makes them an increasingly attractive alternative to traditional aluminium and steel alloys. Mg alloys possess a unique combination of desirable characteristics, including comparable strength, superior formability, excellent cast ability, and ease of machining, recyclability, high damping capacity, and impressive weight-to-stiffness and weight-to-strength ratios. These advantageous properties position Mg alloys as strong contenders against aluminium alloys in a wide range of industrial and commercial applications [1-4].

The development of magnesium alloys can be divided into four clear phases: an initial 80-year period focused on foundational research, followed by 40 years of semi-technical progress, and then 30 years of widespread commercial and industrial adoption. Currently, Mg alloys have become ubiquitous across diverse industries, such as pharmaceuticals, medical equipment, industrial engineering, and scientific research, despite persistent challenges necessitating continued innovation and advancement [5].

Numerous fabrication processes are utilized in the production of magnesium alloys and magnesium metal matrix composites, demonstrating their versatility and capacity to adapt to diverse application requirements. Furthermore, attaining the desired dispersion of enhancing particles in surface composites through conventional methods has been recognized as a challenging endeavor. This establishes the significance of this issue [6-7]. Over the past decade, various efforts have been made to address these limitations. Conventional surface treatments have been employed to distribute ceramic-based particles on metallic surfaces, but with limited success [8-12]. The formation of unfavourable phases during the fabrication of surface composites was a concern with liquid processing [13-15].

Surface composites represent a promising solution to address these limitations. By incorporating reinforcement particles into the surface layer of a material, surface composites significantly enhance properties such as hardness, wear resistance, and fatigue life while retaining the desirable bulk characteristics of the base material. Silicon carbide (SiC) is a commonly used reinforcement material due to its high hardness, thermal stability, and chemical inertness. Combining Mg alloy AZ31B with SiC reinforcement particles has the potential to create a surface composite with superior mechanical and tribological properties [16].

Friction Stir Processing (FSP) is a solid-state technique derived from Friction Stir Welding (FSW). It has emerged as an efficient and versatile method for fabricating surface composites. FSP involves the localized plastic deformation of a material using a rotating tool that generates heat through friction, softening the material without melting it. This process facilitates the incorporation of reinforcement particles into the surface layer of the substrate [17].

The research conducted by Del Valle et al. [18] and Zang et al. [19] explored the impact of Friction Stir Processing on AZ31 magnesium alloys, reporting substantial grain refinement. In present work they were able to achieve a remarkably fine grain size of approximately 0.5 micrometers, which enabled superplastic behavior at elevated temperatures. Similarly, Zang et al. observed grain size variations ranging from 10.4 micrometers to 13.6 micrometers across multiple FSP passes, demonstrating the process's capability to control the evolution of the microstructure. Raja et al. [20] and Panigrahi et al. [21] studied the effects of Friction Stir Processing on other magnesium alloys, including AZ91 and QE22. Raja et al. observed that the initial dendritic alpha-phase magnesium structure, measuring 100 micrometers, was refined down to 2 micrometers. Similarly, Mohan & Panigrahi investigated the high-temperature tensile deformation behavior of QE22 alloys, highlighting the dual-mode superplastic characteristics exhibited by these materials. Numerous studies have documented the enhancement of mechanical properties through Friction Stir Processing. Sing et al. [22] reported a 29% increase in tensile strength and a 33% improvement in creep strength for AZ91 magnesium alloys at room temperature. These strength gains were further amplified at elevated temperatures. Similarly, Shang et al. [23] demonstrated that introducing extension twins in AZ31 alloys increased the yield strength from 96 MPa to 122 MPa. Moreover, Patel et al. [24] achieved an 80% increase in hardness and a 24% improvement in tensile strength by incorporating a copper backing plate during the FSP process.

Magnesium alloys are extensively utilized across a wide range of industries due to their inherent lightweight nature and superior mechanical properties. They play a crucial role in a multitude of applications, including components for braking systems, clutch mechanisms, transmission housings, aircraft landing gear, helicopter rotor assemblies, gearbox casings, and high-speed textile machinery [25] [26] [27]. Furthermore, these alloys are commonly incorporated into consumer goods such as luggage, hand tools, computer casings, and ladders. In the electronics sector, magnesium alloys and their composite counterparts are the preferred materials for manufacturing device housings, packaging materials, hard disk arms, and mobile phone enclosures, leveraging their advantageous strength-to-weight ratio and durability [28]. The low density and high strength of these alloys make them well-suited for applications requiring dynamic loading, while their exceptional heat dissipation, electromagnetic shielding, and minimal radio frequency interference offer additional benefits [29].

Magnesium alloys have gained recognition in the biomedical sector, where they are employed in cardiovascular stents, orthopaedic implants, and wheelchair components, leveraging their biocompatibility and biodegradable nature [30]. However, limited mechanical strength and high degradation rates constrain their broader adoption. Although integrated into automotive applications in vehicles like Jeep, Mercedes-Benz, Ford light trucks, and Renault 18 Turbo, their relatively low strength and plasticity have impeded widespread use in large-scale manufacturing [31]. To address these limitations, surface modification techniques, such as coatings and reinforcements, can enhance the strength, ductility, and corrosion resistance of magnesium alloys, enabling them to better compete with conventional materials across various industrial applications [17].

The groove method is a specific approach within FSP used for surface composite fabrication. In this technique, grooves are machined into the surface of the base material and filled with reinforcement particles before undergoing FSP. The rotating tool stirs the particles into the substrate, creating a homogeneously reinforced surface layer. The groove method is advantageous for its ability to achieve uniform particle dispersion and a strong metallurgical bond between the substrate and reinforcement particles.

The demand for lightweight and high-performance materials in various engineering applications underscores the importance of optimizing surface modification techniques for Mg alloys. Despite the proven benefits of FSP and the groove method for surface composite fabrication, several challenges remain [32]. These include achieving uniform dispersion of reinforcement particles, minimizing defects, and optimizing process parameters to maximize the mechanical and tribological performance of the modified surface [33].

Process parameters such as tool rotational speed, traverse speed, groove geometry, and the volume fraction of reinforcement particles play a critical role in determining the quality of the surface composite.

The existing literature suggests that substantial research has been conducted on aluminium-based composites fabricated through friction stir processing with various particle reinforcements using the groove method. Therefore, it is essential to investigate magnesium-based alloy materials, as they possess less number of literatures for mg alloy AZ31B compared to other matrix materials, making them suitable for a wide range of applications. This study examines the processing of 6 mm-thick magnesium alloy AZ31B-based metal matrix composite plates using friction stir processing. The aim is to fabricate an AZ31B-SiC composite and modify the surface through friction stir processing with the groove method. An L9 orthogonal array with four factors and three levels was employed during the friction stir processing [34]. The investigation focuses on analysing key mechanical properties, including ultimate tensile strength, yield strength, and microhardness. Additionally, the microstructural characteristics were observed and recorded using optical microscopy and scanning electron microscopy to provide deeper insights into the surface composite [35]. This work offers a comprehensive overview of the microstructural changes and the impact of the proposed approach on the AZ31B-SiC surface composite.

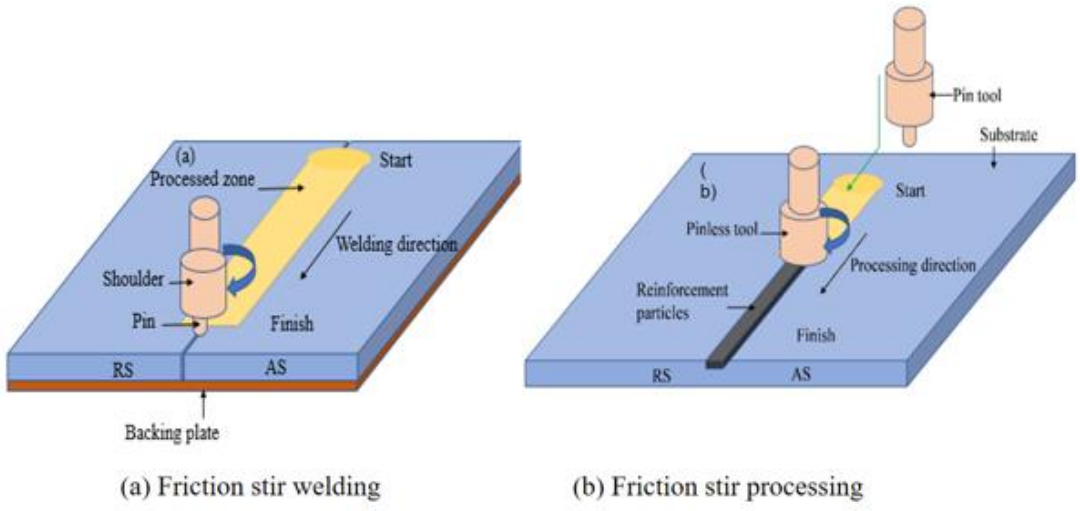

Figure 1 (a) Friction Stir Welding, (b) Friction Stir Processing

Experimental details

This section outlines the materials and methods employed in the study. It covers the procurement of the materials used in the experiments and the general approaches adopted for sample preparation, as detailed in the reviewed literature.

Material Procurement

The materials employed in this study were meticulously chosen to ensure their suitability for friction stir processing. The magnesium alloy AZ31B, widely recognized for its exceptional mechanical characteristics and corrosion resistance, was procured in the form of 6 mm thick sheets. These sheets were sourced from a certified supplier, ensuring compliance with ASTM standards and verification of the chemical composition and mechanical properties through comprehensive material test certificates.

Furthermore, silicon carbide particles were selected as the reinforcement material due to their exceptional hardness and wear resistance properties. These reinforcing particles were procured in a powder form, with an average particle size in the nanometer range, from a certified supplier of high-purity (99%) silicon carbide powder.

Methodology for sample preparation

This work offers a thorough examination of the mechanical characteristics, including strength and hardness, of magnesium alloy and silicon carbide reinforced surface composites. The findings provide valuable insights that can inform the development of materials optimized for applications demanding exceptional mechanical performance.

This study aims to fabricate surface composites composed of a magnesium alloy matrix reinforced with silicon carbide particles using the friction stir processing a groove method. Additionally, this work advances the state of the art for manufacturing surface composites by incorporating nano-scale SiC reinforcement, which is expected to lead to enhanced mechanical properties and improved overall performance of the surface-modified material. The study utilized square plates of AZ31B magnesium alloy, a material commonly employed in aerospace applications. These plates, measuring 100 x 100 mm2 and with a thickness of 6 mm, were prepared using wire-cut electrical discharge machining. Within the base plate, grooves with a depth of 4.5 mm and varying widths were created, as shown in Figure 2. For further analysis, the groove widths were set to 0.26 mm, 0.58 mm, and 1.032 mm.

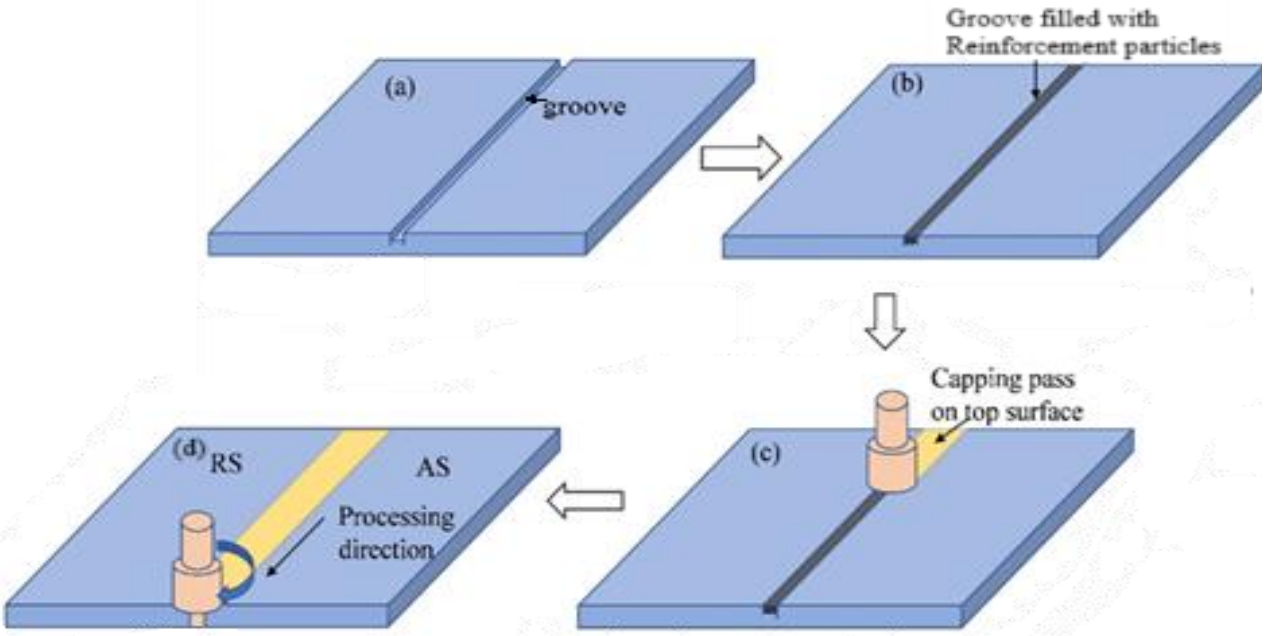

Figure 2 Sample Preparation (a) Groove on top of Plate, (b) Groove filled with Reinforcement particles, (c) Capping pass on top Surface, (d) Friction stir Processing pass.

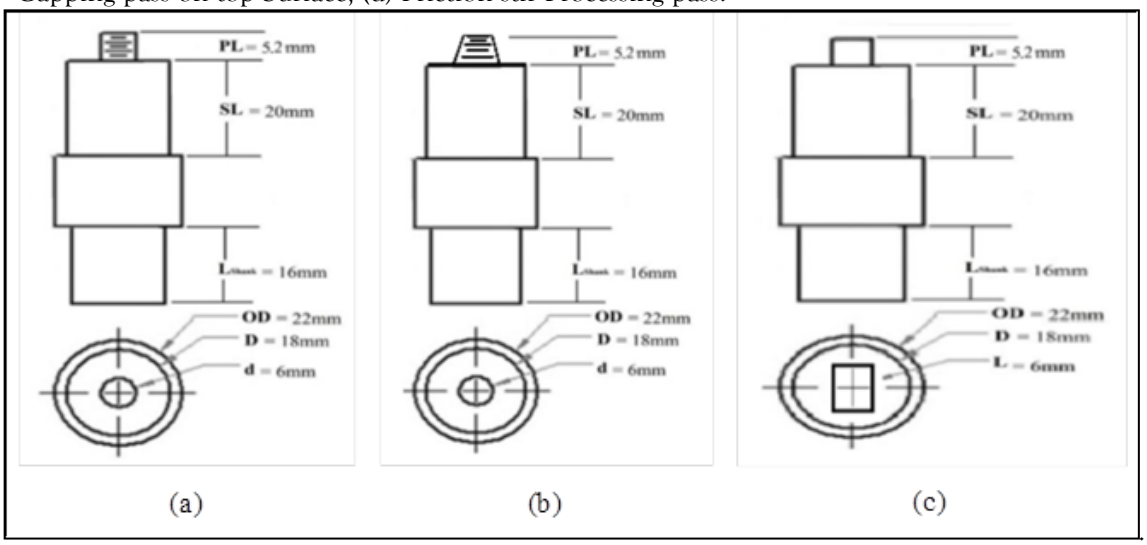

Figure 3 Tool pin profile: (a) Cylindrical threaded, (b) Taper threaded, (c) Square headed

Further fabricated custom FSP tools from high-strength H13 tool steel, featuring three distinct geometries: square, tapered, and tapered threaded, as illustrated in Figure 3. These tools were manufactured at a specialized machining facility to ensure precise dimensions and optimal performance during the processing phase. The selected materials and tools were thoroughly prepared and characterized to meet the specific requirements of the experimental setup

Design of experiment

A total of 9 experimental trials were conducted using an L9 orthogonal array design, wherein four factors were investigated at three distinct levels each. The factors and their respective levels are summarized in Table 1:

Tool geometry: square, cylindrical threaded, and tapered threaded

Rotational speed: 545 rpm, 765 rpm, and 1070 rpm

Traverse speed: 20 mm/min, 31.5 mm/min, and 50 mm/min

Groove width: 0.26 mm, 0.58 mm, and 1.032 mm.

For all experiments, the groove depth was maintained at a constant 4.5 mm.

The samples were prepared by cutting the processed plates into suitable dimensions for conducting various characterization tests, including tensile, hardness, and microstructural evaluation. The mechanical properties, such as tensile strength, yield strength, and elongation, were assessed using a universal testing apparatus. Vickers hardness measurements were performed on the surface of the composite materials. Comprehensive microstructural examination, utilizing optical and scanning electron microscopy techniques, was carried out to investigate the distribution and dispersion of the SiC reinforcement within the Mg alloy matrix.

Table 1 L9 orthogonal array for Groove method

Exp. No	Tool Rotation Speed (RPM)	Traverse speed (mm/min)	Groove width (mm)	Tool Profile
S1	545	20	0.26	Tapered Threaded
S2	545	31.5	0.58	Square Head
S3	545	50	1.032	Cylindrical Threaded
S4	765	20	0.58	Cylindrical Threaded
S5	765	31.5	1.032	Tapered Threaded
S6	765	50	0.26	Square Head
S7	1070	20	1.032	Square Head
S8	1070	31.5	0.26	Cylindrical Threaded
S9	1070	50	0.58	Tapered Threaded

Material characterization

In the present study, various mechanical characterization techniques were employed to analyze the influence of process parameter variations. Uniaxial tensile tests were conducted in accordance with ASTM E8-E8M [36] to determine the mechanical properties, including yield stress, ultimate tensile stress, and elongation, of the surface composite samples measuring 100 mm x 10 mm x 6 mm. These samples were analyzed using a universal testing machine with a capacity of 100 KN and a test speed of 1 mm/min at the Hertz Testing and Training Center in Ahmedabad. Additionally, the hardness of the Mg alloy AZ31B and SiC-reinforced surface composite was evaluated using a Vickers hardness testing machine, as per ASTM E92-17 [37] standards, on samples measuring 50 mm x 6 mm x 3 mm.

Comprehensive microstructural characterization of magnesium alloy and silicon carbide reinforcement surface composites, utilizing techniques such as Optical Microscopy and Field Emission Scanning Electron Microscopy, offers valuable insights into the distribution and orientation of the nanoscale reinforcing particles within the processed region. This knowledge is essential for assessing the quality of the magnesium alloy and silicon carbide reinforcement surface composites and ensuring the effective dispersion of the nano-scale reinforcements.

Results and Discussion

This section examines the effects of the process parameters—rotational speed, feed rate, groove width, and tool pin profile type—on the response variables. Comparisons are made for specific levels of each parameter, and an overall optimization is discussed.

Effect of process parameters on Mechanical Properties

Effect of Tool Rotation Speed

The tool's rotational speed substantially influences heat generation, material flow, and mechanical characteristics in friction stir processing. Insufficient heat is produced at lower rotational speeds, resulting in poor bonding, whereas excessive speeds may cause overheating, grain growth, and reduced strength. The mechanical properties of the Mg Alloy processed at various tool rotational speeds are presented in Table 2, Table 3, and Table 4, with their graphical representations depicted in Figure 4, Figure 5, and Figure 6.

Effect of tool rotational speed 545 RPM

At 545 RPM (Table 2, Figure 4), the highest ultimate tensile strength recorded is 152.37 MPa, while the lowest is 123.52 MPa. The percent elongation ranges between 3.15% and 5.99%, with specimen S2 showing the highest ductility. The hardness of the specimens varies, with S2 achieving the highest hardness of 100.54 HV, indicating improved grain refinement and strengthening at this rotational speed. The UTS of specimen S2 is 23.3% higher than S1, suggesting that optimal heat generation and material mixing occur at 545 RPM.

Table 2 Mechanical properties at 545 RPM tool rotational speed

Specimen Number	UTS	POE	Avg. Hardness
S1	123.5197	4.033333	73.13636
S2	152.367	5.996667	100.5364
S3	141.3873	3.153333	72.04545

Additionally, S3 exhibits a 12.7% increase in UTS compared to S1, demonstrating intermediate mechanical strength. The hardness of S2 is 37.5% higher than S1, further supporting the notion of better grain refinement and strengthening at this rotational speed.

International Journal of Environmental Sciences
ISSN: 2229-7359
Vol. 11 No. 14s 2025
https://www.theaspd.com/ijes.php

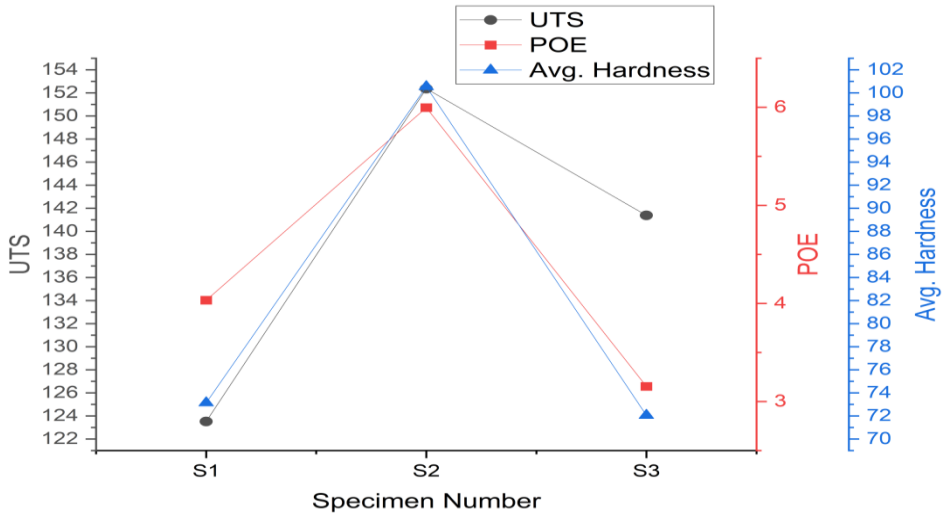

Figure 4: Graphical representation of Mechanical properties at 545 RPM tool rotational speed

Effect of tool rotational speed 765 RPM

Elevating the tool rotational speed to 765 RPM (Table 3, Figure 5) results in a diminished ultimate tensile strength, with the maximum value decreasing to 140.722 MPa, approximately 7.6% lower than the peak UTS at 545 RPM. Conversely, hardness exhibits a slight increase, with specimen S6 displaying a hardness of 94.86 HV, which is 5.3% higher than S3 at 545 RPM.

Table 3 Mechanical properties at 765 RPM tool rotational speed

Specimen Number	UTS	POE	Avg. Hardness
S4	111.7557	3.16	75.6
S5	71.23533	2.2	73.32727
S6	140.722	4.36	94.86364

When the rotational speed is escalated to 765 RPM (Table 3, Figure 5), a noticeable reduction in UTS is observed. Specifically, specimen S6 demonstrates a 7.6% decrease in UTS compared to S2 at 545 RPM, while specimen S5 showcases a significant 53.3% reduction in UTS, suggesting poor material consolidation. However, specimen S6 achieves a hardness of 94.86 HV, which is 5.3% higher than S3 at 545 RPM, indicating improved hardness at this elevated rotational speed.

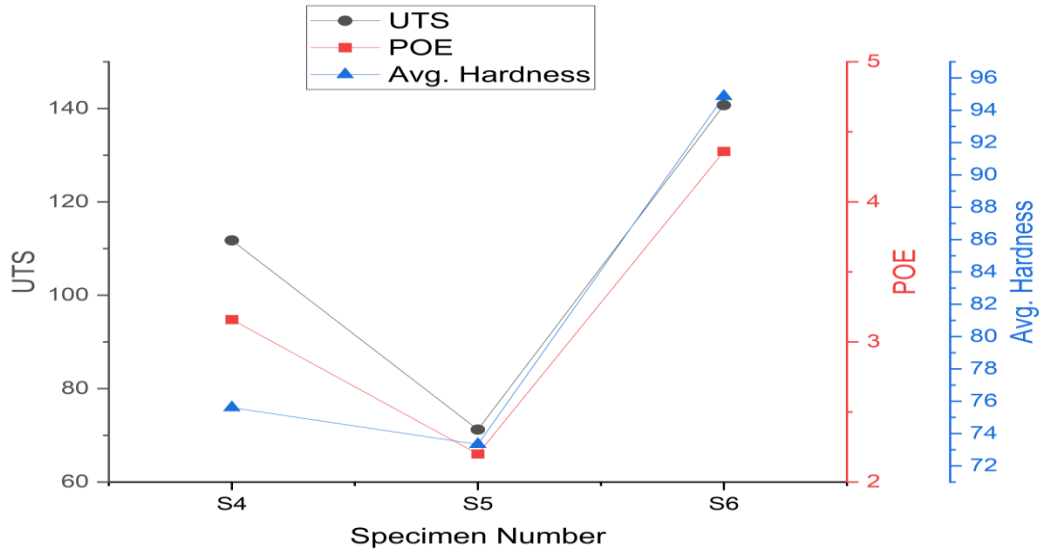

Figure 5: Graphical representation of Mechanical properties at 765 RPM tool rotational speed

Effect of tool rotational speed 1070 RPM

At 1070 RPM (Table 4, Figure 6), a further decline in ultimate tensile strength is observed. Specimen S8 exhibits the highest UTS at this speed, measuring 123.34 MPa, which is 19.1% lower than the peak UTS recorded at 545 RPM. Additionally, hardness values show a slight increase, with specimen S9 achieving a hardness of 91.76 HV.

International Journal of Environmental Sciences
ISSN: 2229-7359
Vol. 11 No. 14s 2025
https://www.theaspd.com/ijes.php

Table 4 Mechanical properties at 1070 RPM tool rotational speed

Specimen Number	UTS	POE	Avg. Hardness
S7	53	2.933333	76.40909
S8	123.347	3.16	80.49091
S9	97.32433	3.773333	91.76364

The decrease in UTS at these elevated rotational speeds suggests that excessive heat input leads to grain coarsening, which in turn diminishes the overall mechanical strength. Specifically, S8 displays a 19.1% reduction in UTS compared to S2 at 545 RPM, while S9 demonstrates an even more significant 31.7% decrease in UTS relative to S2. Despite the relatively stable hardness values, the excessive rotational speed of 1070 RPM appears to promote grain growth, resulting in a decline in the overall mechanical properties.

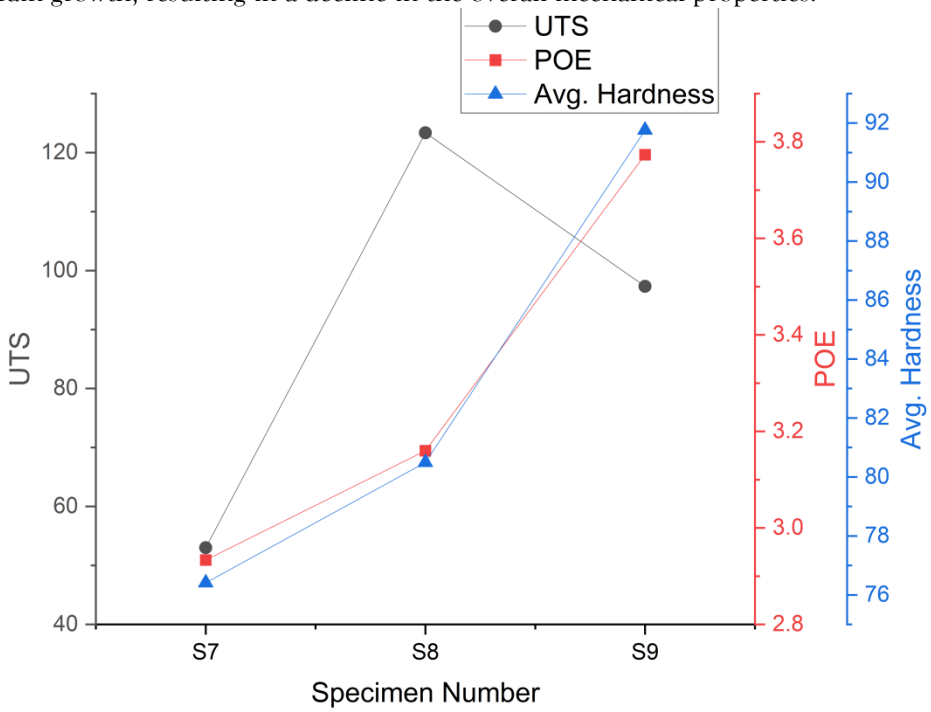

Figure 6: Graphical representation of Mechanical properties at 1070 RPM tool rotational speed

The optimal tool rotational speed for achieving the maximum ultimate tensile strength and hardness was found to be 545 RPM. Increasing the rotational speed to 765 RPM resulted in a slight improvement in hardness, but a reduction in tensile strength. Further increasing the rotational speed to 1070 RPM caused a significant decrease in UTS, which was attributed to grain growth. The 545 RPM rotational speed provided the highest UTS and hardness values. Specifically, the UTS decreased by 7.6% when the speed was increased to 765 RPM, and by 19.1% when it was increased to 1070 RPM. These findings suggest that higher rotational speeds promote grain growth, ultimately diminishing the mechanical properties of the material.

Effect of Feed rate

Feed rate is a critical parameter that governs strain rate and heat input during the process. A lower feed rate facilitates improved material bonding, but may also lead to excessive heat generation. Conversely, a higher feed rate can result in insufficient heat input, ultimately causing defects. The mechanical characteristics associated with varying feed rates are presented in the tabular formats of Tables 5, 6, and 7, and their corresponding graphical representations are depicted in Figures 7, 8, and 9.

Effect of Feed rate 20 mm/min

At 20 mm/min (Table 5, Figure 7), the ultimate tensile strength ranges from 53 MPa to 123.52 MPa. The lowest recorded UTS value for specimen S7 suggests incomplete material mixing at this lower feed rate. The hardness measurements are relatively moderate, with S7 exhibiting a hardness of 76.40 HV.

Table 5 Mechanical properties at 20 mm/min feed rate

Specimen Number	UTS	POE	Avg. Hardness
S1	123.5197	4.033333	73.13636

International Journal of Environmental Sciences
ISSN: 2229-7359
Vol. 11 No. 14s 2025
https://www.theaspd.com/ijes.php

S4	111.7557	3.16	75.6
S7	53	2.933333	76.40909

The highest UTS recorded at 20 mm/min (Table 5, Figure 7) is 123.52 MPa, while the lowest is 53 MPa. This indicates that specimen S1 displays UTS that is 133.1% higher than S7, confirming that lower feed rates may not provide adequate bonding in all cases.

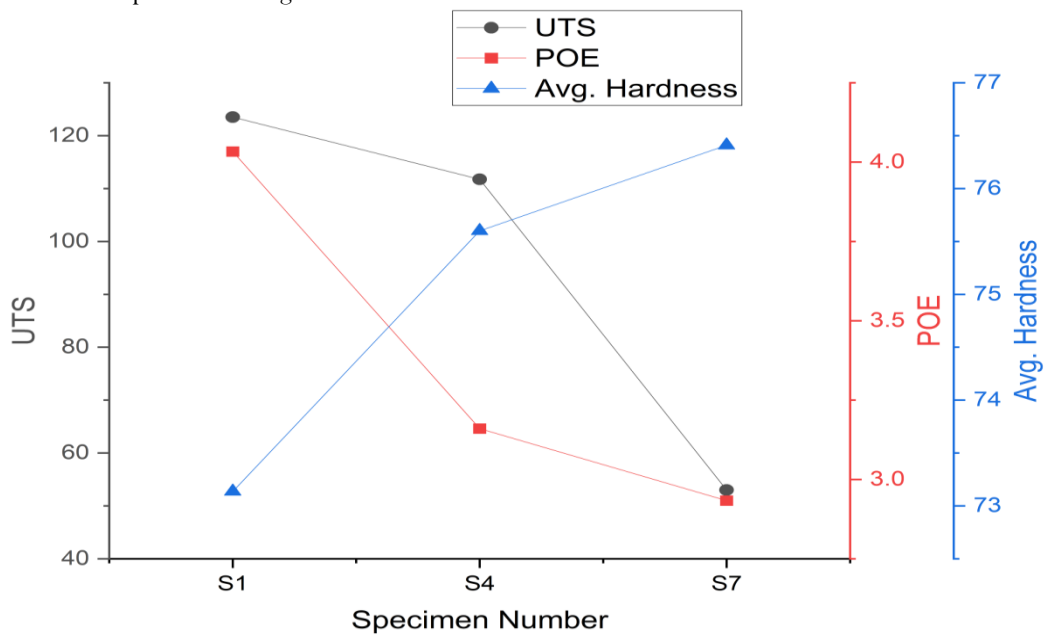

Figure 7: Graphical representation of Mechanical properties at 20 mm/min feed rate

Effect of Feed rate 31.5 mm/min

Increasing the feed rate to 31.5 mm/min (Table 6, Figure 8) significantly boosts the ultimate tensile strength. Specimen S2 reaches a UTS of 152.37 MPa, a 23.3% increase compared to the 20 mm/min feed rate. Similarly, the hardness values also improve, with S2 achieving a hardness of 100.54 HV.

Table 6 Mechanical properties at 31.5 mm/min feed rate

Specimen Number	UTS	POE	Avg. Hardness
S2	152.367	5.996667	100.5364
S5	71.23533	2.2	73.32727
S8	123.347	3.16	80.49091

At the 31.5 mm/min feed rate (Table 6, Figure 8), there is a noticeable enhancement in UTS. Specifically, S2 attains a UTS of 152.37 MPa, which is 23.3% higher than S1 at 20 mm/min. Additionally, the hardness values show a 37.5% improvement for S2 compared to S1.

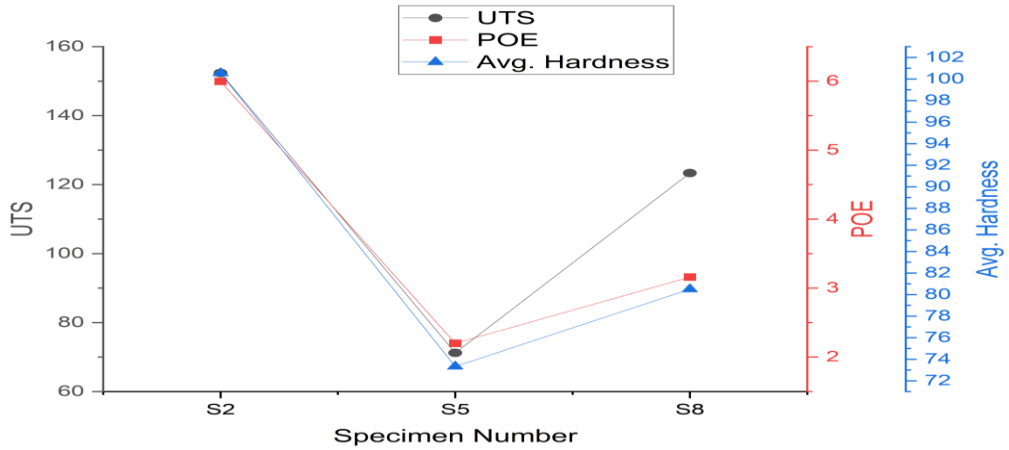

Figure 8: Graphical representation of Mechanical properties at 31.5 mm/min feed rate

Effect of Feed rate 50 mm/min

International Journal of Environmental Sciences
ISSN: 2229-7359
Vol. 11 No. 14s 2025
https://www.theaspd.com/ijes.php

At a feed rate of 50 mm/min (Table 7, Figure 9), the ultimate tensile strength slightly decreases to 141.38 MPa, indicating that an excessively high feed rate might compromise the quality of material bonding. The hardness values exhibit a similar trend, with the highest value recorded at 94.86 HV.

Table 7 Mechanical properties at 50 mm/min feed rate

Specimen Number	UTS	POE	Avg. Hardness
S3	141.3873	3.153333	72.04545
S6	140.722	4.36	94.86364
S9	97.32433	3.773333	91.76364

The data presented in Table 7 and Figure 9 shows a reduction in UTS at the 50 mm/min feed rate. Specifically, specimen S3 records UTS of 141.38 MPa, which is 7.2% lower than that of specimen S2 at the 31.5 mm/min feed rate. This suggests that an excessive feed rate can reduce the effectiveness of material bonding, ultimately leading to lower mechanical strength.

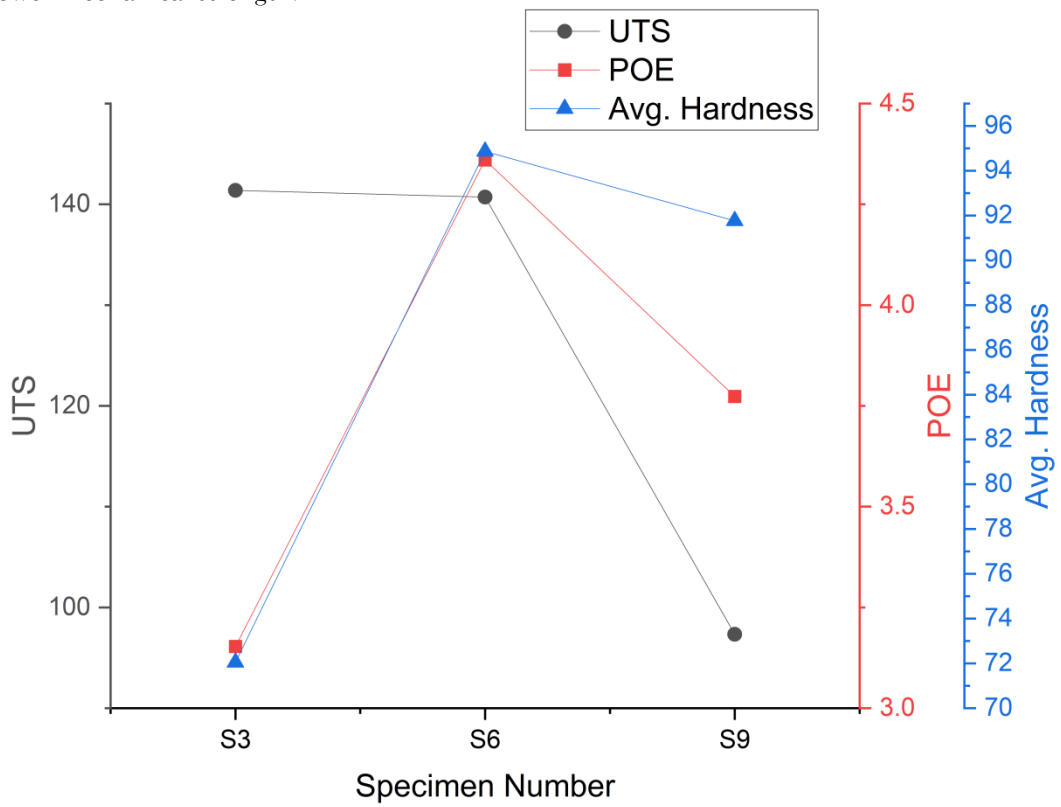

Figure 9: Graphical representation of Mechanical properties at 50 mm/min feed rate

The analysis indicates that the optimal feed rate for maximizing ultimate tensile strength and hardness is 31.5 mm/min. By increasing the feed rate beyond this point results in a slight decrease in UTS, likely due to insufficient heat input. The UTS exhibited a 23.3% increase when the feed rate was increased from 20 mm/min to 31.5 mm/min. By increasing the feed rate further to 50 mm/min, however, resulted in a 7.2% decline in UTS. These findings suggest that 31.5 mm/min is the optimal feed rate for achieving the highest UTS and hardness values.

Effect of Groove width

The groove width created during the friction stir processing significantly impacts the material flow and distribution of the reinforcement, which in turn affects the mechanical properties, such as ultimate tensile strength, percentage of elongation, and average hardness. The experimental findings for groove widths of 0.26 mm, 0.58 mm, and 1.032 mm are presented in the corresponding tables, and their graphical representations are shown in Figures 10, 11, and 12.

Effect of Groove width 0.26 mm

The mechanical properties for a groove width of 0.26 mm, as presented in Table 8, show that specimen S6 had the highest ultimate tensile strength of 140.722 MPa, while specimens S1 10 suggests that at this groove width, the material flow was sufficient to improve and S8 exhibited relatively lower values. The percent elongation ranged from 3.16 to 4.36, and the hardness values varied from 73.136 HV to 94.863 HV. The graphical representation in Figure mechanical properties, but did not achieve optimal reinforcement dispersion.

Table 8 Mechanical properties at 0.26 mm groove width

International Journal of Environmental Sciences
ISSN: 2229-7359
Vol. 11 No. 14s 2025
https://www.theaspd.com/ijes.php

Specimen Number	UTS	POE	Avg. Hardness
S1	123.5197	4.033333	73.13636
S6	140.722	4.36	94.86364
S8	123.347	3.16	80.49091

Analysis of Table 8 and Figure 10 for the 0.26 mm groove width reveals that specimen S6 had the highest UTS, which was 14% higher than S1 and 0.14% higher than S8. Additionally, the POE increased by 37.97% in S6 compared to S8, while the hardness also showed a 29.70% increase, indicating improved material properties due to better reinforcement dispersion.

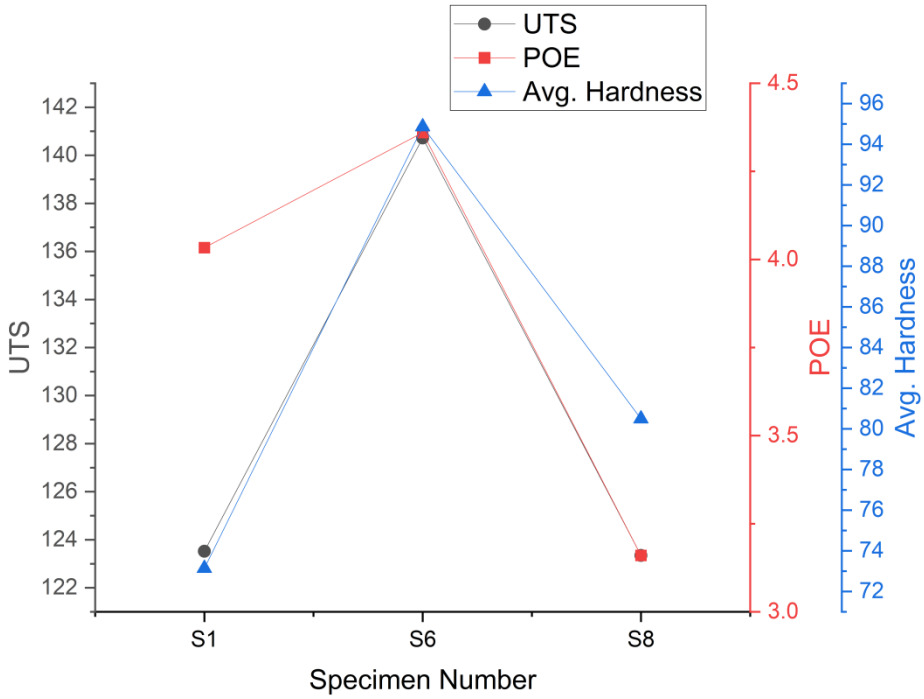

Figure 10: Graphical representation of Mechanical properties at 0.26 mm groove width

Effect of Groove width 0.58 mm

The results presented in Table 9 and Figure 11 indicate that increasing the groove width to 0.58 mm led to a significant enhancement in the mechanical properties of the material. Specimen S2 exhibited the highest ultimate tensile strength and percentage of elongation, while the hardness reached 100.536 HV. The graphical representation further corroborates that this groove width facilitated a more uniform distribution of the reinforcement, resulting in improved mechanical performance. However, some specimens, such as S4 and S9, displayed reduced UTS values, suggesting that further optimization of the process parameters may be required to achieve consistent improvements across all samples.

Table 9 Mechanical properties at 0.58 mm groove width

Specimen Number	UTS	POE	Avg. Hardness
S2	152.367	5.996667	100.5364
S4	111.7557	3.16	75.6
S9	97.32433	3.773333	91.76364

Overall, the 0.58 mm groove width provided the best overall results. Specimen S2 achieved the highest UTS, which was a 56.57% increase compared to S9, and the POE increased by 89.72%, indicating superior ductility. The hardness values were also the highest, reaching 100.536 HV, representing a 32.98% improvement over S9.

International Journal of Environmental Sciences
ISSN: 2229-7359
Vol. 11 No. 14s 2025
https://www.theaspd.com/ijes.php

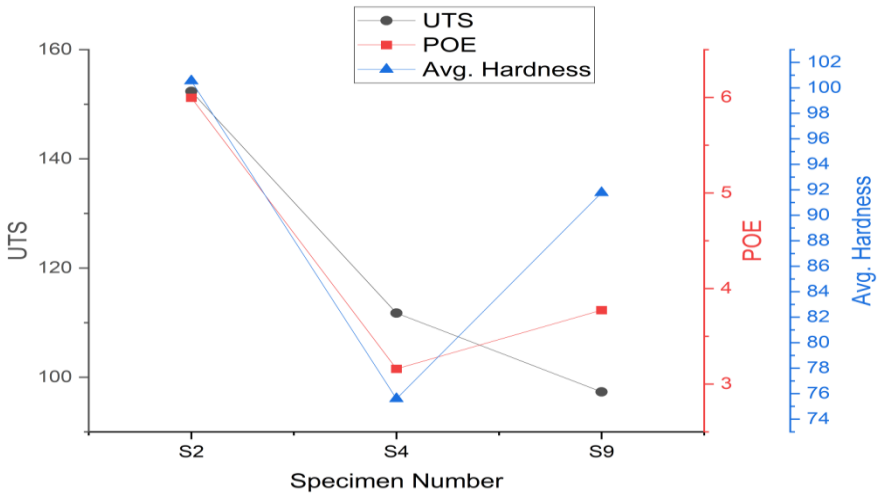

Figure 11: Graphical representation of Mechanical properties at 0.58 mm groove width

Effect of Groove width 1.032 mm

Increasing the groove width to 1.032 mm, as shown in Tabl 10, led to a decline in the mechanical properties of the material. Specimen S3 exhibited the highest ultimate tensile strength, while specimens S5 and S7 displayed lower UTS values (71.235 MPa and 53 MPa, respectively). Furthermore, the hardness values ranged between 72 and 76 HV, as illustrated in Figure 12. This decline in mechanical properties suggests that an excessively wide groove width may result in poor bonding and uneven distribution of the reinforcement.

Table 10 Mechanical properties at 1.032 mm groove width

Specimen Number	UTS	POE	Avg. Hardness
S3	141.3873	3.153333	72.04545
S5	71.23533	2.2	73.32727
S7	53	2.933333	76.40909

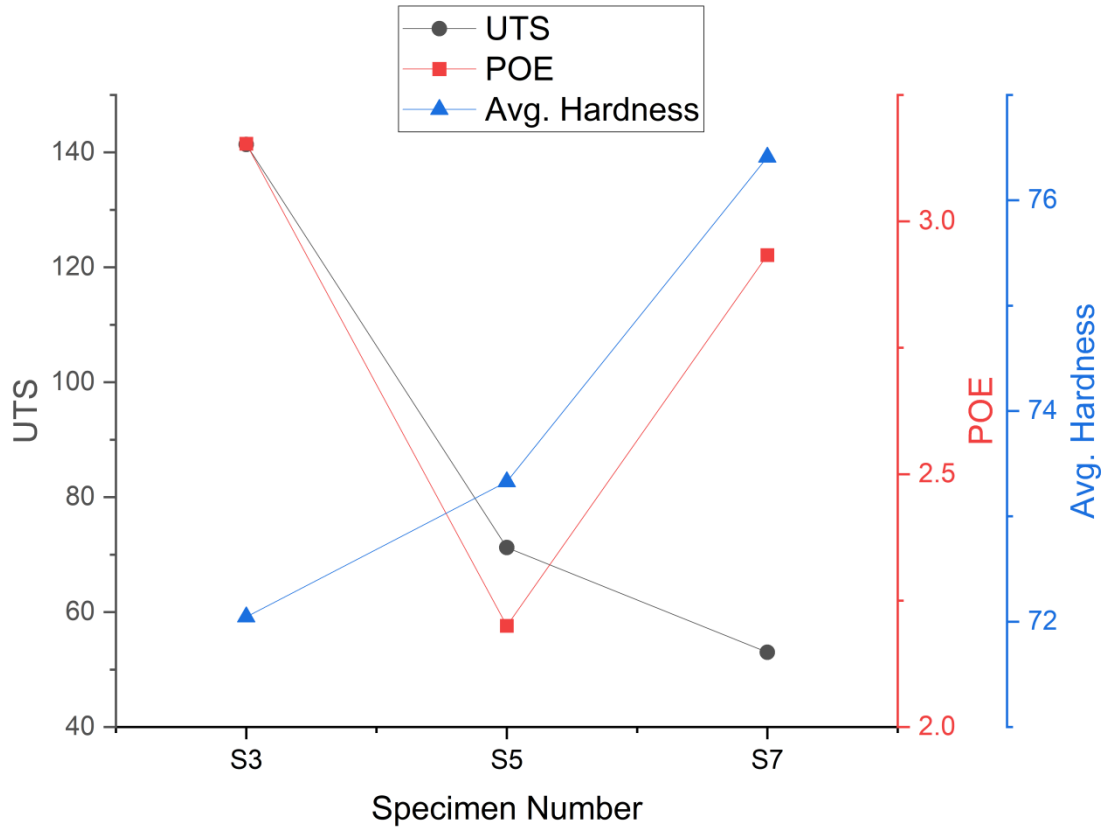

Figure 12: Graphical representation of Mechanical properties at 0.1.032 mm groove width

When the groove width was further increased to 1.032 mm, a reduction in the overall mechanical performance was observed. Although specimen S3 had the highest UTS, this value was 165.7% higher than S7, but still lower than

the performance of specimen S2 from the 0.58 mm groove width group. The hardness values showed only a minor 6.05% increase compared to S7, indicating that the excessive groove width led to poor reinforcement dispersion, ultimately decreasing the mechanical properties.

The findings suggest that a groove width of 0.58 mm facilitated the optimal mechanical performance, as this configuration demonstrated the highest ultimate tensile strength, percentage of elongation, and hardness values across the tested conditions. This can be attributed to the enhanced dispersion of the SiC reinforcement within the Mg matrix, highlighting the advantages of achieving a uniform distribution of the reinforcing phase.

Effect of Tool Pin Profile

The shape of the tool pin plays a crucial role in determining the efficiency of material mixing and the dispersion of the reinforcement during the friction stir processing operation. Three distinct pin profiles were evaluated, including Tapered Threaded, Square Headed, and Cylindrical Threaded, and their corresponding mechanical properties are summarized in the respective tables (11, 12, and 13) and illustrated in the corresponding figures (13, 14, and15).

Effect of Tool Pin Profile Tapered Threaded

The analysis of the tapered threaded pin profile presented in Table 11 indicates moderate mechanical properties. Specimen S1 achieved the highest ultimate tensile strength and percentage of elongation of 4.033, while the hardness values ranged between 73.136 HV and 91.763 HV. The graph in Figure 13 suggests that although this profile ensures adequate material flow, it does not result in the highest mechanical strength.

Table 11 Mechanical properties at taper threaded (TT) pin profile

Specimen Number	UTS	POE	Avg. Hardness
S1	123.5197	4.033333	73.13636
S5	71.23533	2.2	73.32727
S9	97.32433	3.773333	91.76364

Table 11 and Figure 13 show that the tapered threaded pin profile provided moderate results. Specimen S1 achieved a UTS of 123.5197 MPa, a 27% increase compared to S5, and hardness improved by 25.18% in S9 compared to S1.

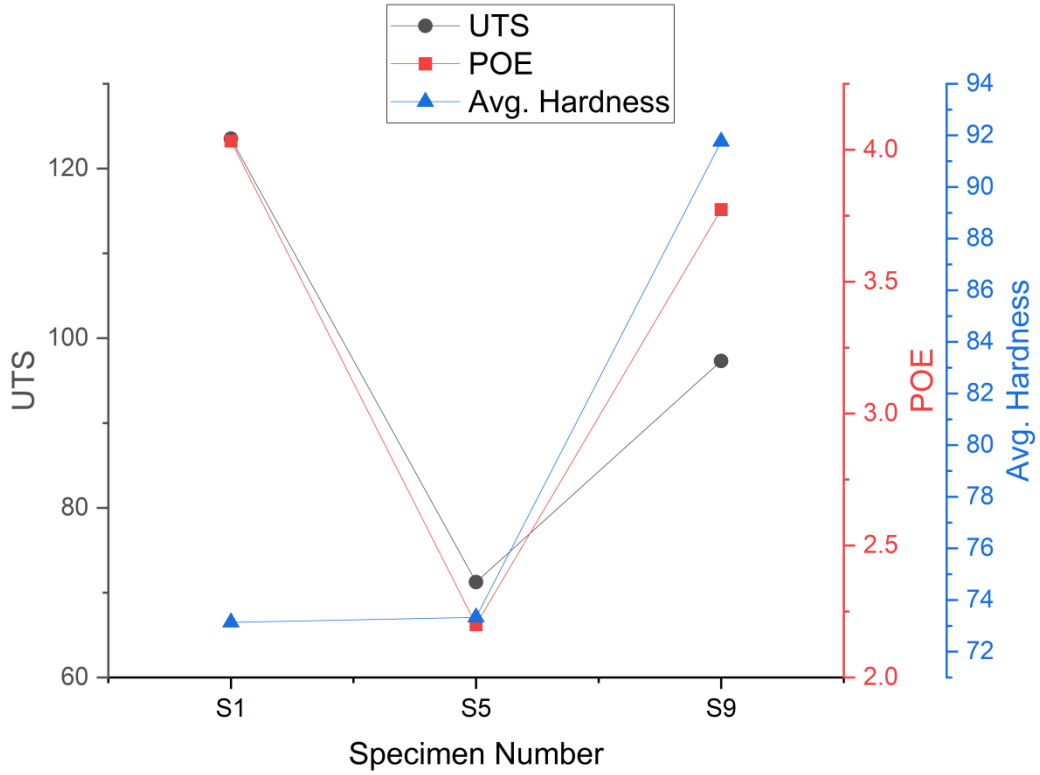

Figure 13: Graphical representation of Mechanical properties at taper threaded (TT) pin profile

In contrast, the square-headed pin profile (Table 12 and Figure 14) demonstrated superior mechanical properties. Specimen S2 achieved the highest UTS, an increase of 187.5% over S7, and the POE increased by 104%, while hardness improved by 32.98%, confirming the superiority of this profile due to its enhanced stirring action and uniform reinforcement dispersion.

Effect of Tool Pin Profile square headed (SQ)

International Journal of Environmental Sciences
ISSN: 2229-7359
Vol. 11 No. 14s 2025
https://www.theaspd.com/ijes.php

The mechanical properties for the square-headed pin profile demonstrate a significant enhancement. Specimen S2 exhibits the highest ultimate tensile strength and percentage of elongation, while the hardness reaches 100.536 HV.

Table 12 Mechanical properties at square headed (SQ) pin profile

Specimen Number	UTS	POE	Avg. Hardness
S2	152.367	5.996667	100.5364
S6	140.722	4.36	94.86364
S7	53	2.933333	76.40909

The graphical representation in Figure 14 further corroborates the superior mechanical performance achieved with this pin profile, which can be attributed to its improved material mixing and uniform reinforcement dispersion.

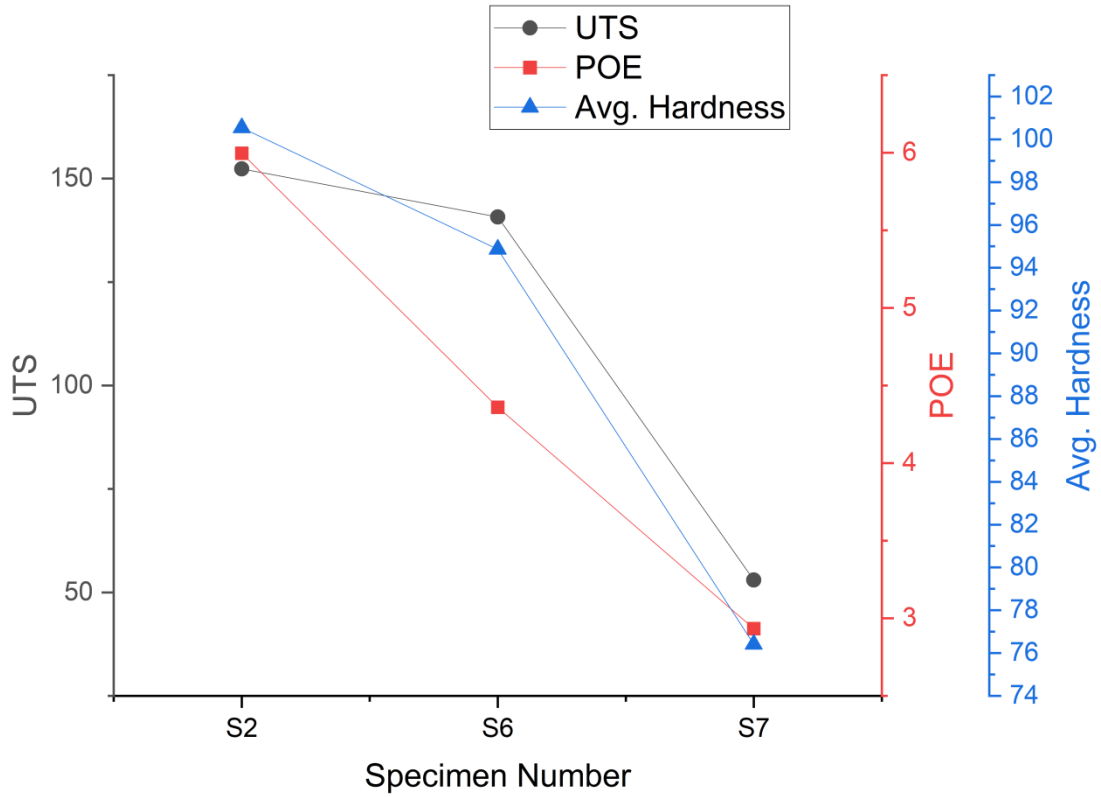

Figure 14: Graphical representation of Mechanical properties at square headed (SQ) pin profile

Effect of Tool Pin Profile cylindrical threaded (TH)

The mechanical properties for the cylindrical threaded pin profile, as presented in Table 13, demonstrate a moderate level of performance. Specimen S3 achieved the highest ultimate tensile strength, while the hardness values ranged from 72.045 HV to 80.490 HV.

Table 13 Mechanical properties at cylindrical threaded (TH) pin profile

Specimen Number	UTS	POE	Avg. Hardness
S3	141.3873	3.153333	72.04545
S4	111.7557	3.16	75.6
S8	123.347	3.16	80.49091

The graphical representation in Figure 15 suggests that this profile facilitates a relatively uniform material mixing, but does not attain the same degree of mechanical enhancement as the square-headed pin profile. The data for the Cylindrical Threaded profile, shown in Table 13 and Figure 15, indicates a moderate performance overall. While specimen S3 exhibited the highest UTS, which was a 26.5% increase over S4, the hardness values were relatively lower, showing only an 11.72% improvement in S8 compared to S3.

International Journal of Environmental Sciences
ISSN: 2229-7359
Vol. 11 No. 14s 2025
https://www.theaspd.com/ijes.php

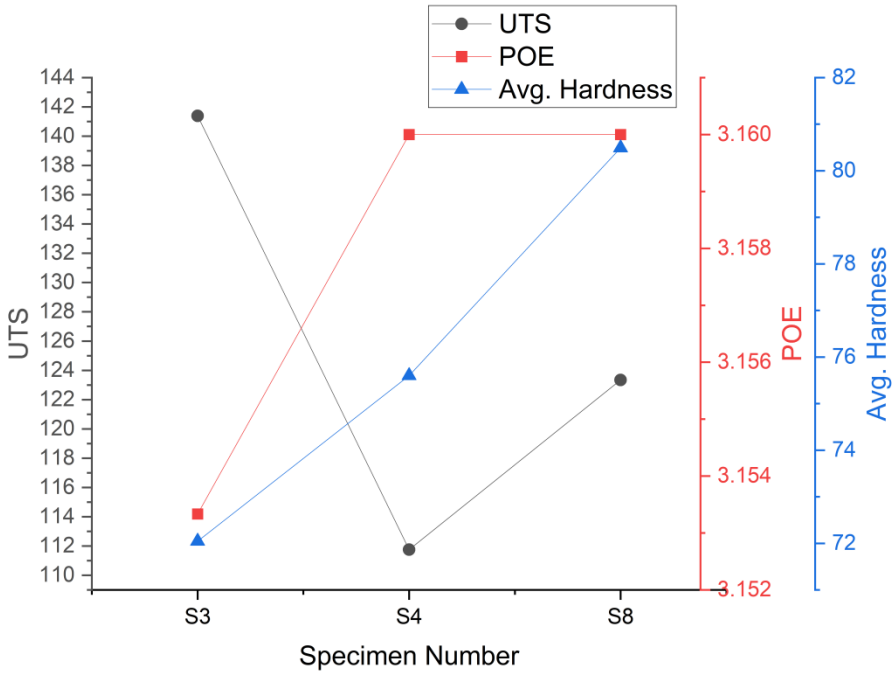

Figure 15: Graphical representation of Mechanical properties at cylindrical threaded (TH) pin profile

The findings indicates that the square-headed pin profile demonstrates the superior mechanical performance, yielding the highest ultimate tensile strength, percentage of elongation, and hardness values across the tested conditions. This suggests that the square-headed pin profile is the most effective tool design for optimizing the mechanical properties of the Mg alloy reinforced with SiC through friction stir processing.

Optical Microscopy and SEM Analysis of Grain Refinement and Particle Distribution

The microstructural evaluation of the Mg AZ31B-SiC surface composite was performed using optical microscopy and scanning electron microscopy (SEM) to analyze grain refinement and reinforcement particle distribution. The results indicate that tool pin profile, rotational speed, traverse speed, and groove width significantly affect reinforcement dispersion and grain refinement in the processed zone.

Optical microscopy to analyze grain refinement and reinforcement particle distribution

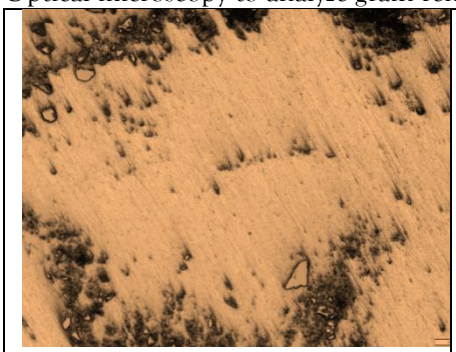

(a) S1: 545 RPM, 20 mm/min, 0.26 mm groove, Tapered Threaded Tool (TT)

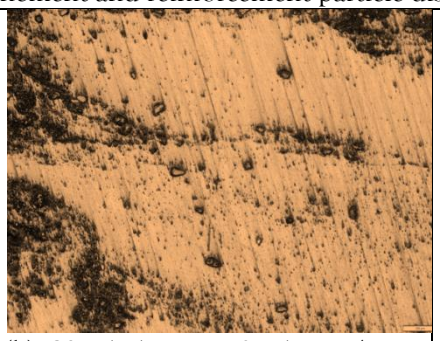

(b) S2: 545 RPM, 31.5 mm/min, 0.58 mm groove, Square Tool (SQ)

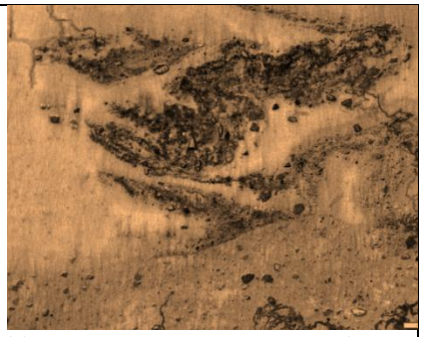

(c) S3: 545 RPM, 50 mm/min, 1.032 mm groove, Cylindrical Threaded Tool (TH)

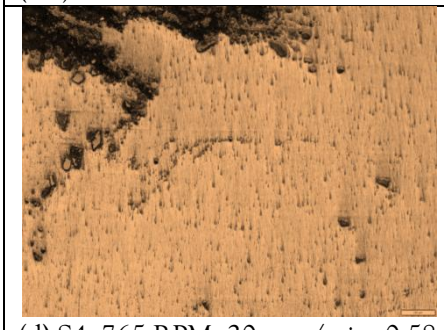

(d) S4: 765 RPM, 20 mm/min, 0.58 mm groove, Cylindrical Threaded Tool (TH)

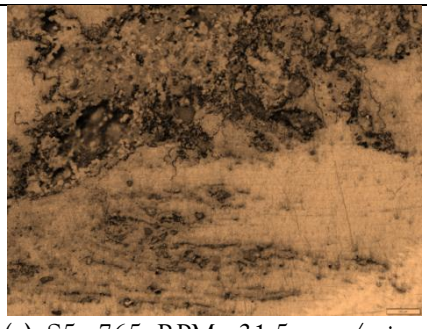

(e) S5: 765 RPM, 31.5 mm/min, 1.032 mm groove, Tapered Threaded Tool (TT)

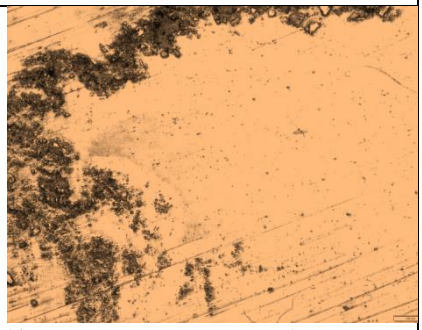

(f) S6: 765 RPM, 50 mm/min, 0.26 mm groove, Square Tool (SQ)

International Journal of Environmental Sciences
ISSN: 2229-7359
Vol. 11 No. 14s 2025
https://www.theaspd.com/ijes.php

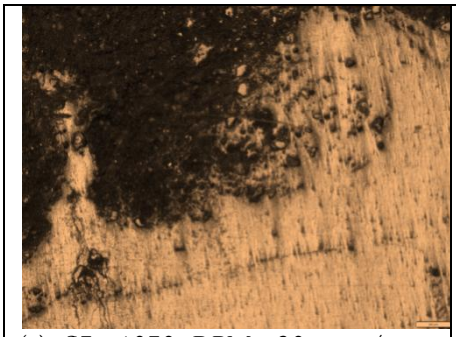

(g) S7: 1070 RPM, 20 mm/min, 1.032 mm groove, Square Tool (SQ)

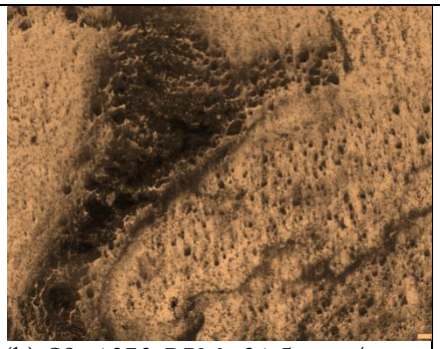

(h) S8: 1070 RPM, 31.5 mm/min, 0.26 mm groove, Cylindrical Threaded Tool (TH)

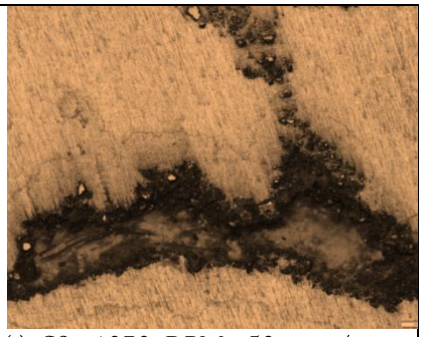

(i) S9: 1070 RPM, 50 mm/min, 0.58 mm groove, Tapered Threaded Tool (TT)

Figure 16 (a-I) Optimal Microstructure and Particle Distribution for Specimen S1 to S9

The SEM analysis Figure 17(a–i) provides insights into SiC particle distribution within the Mg matrix, which directly influences mechanical performance. The optical microscopy (OM) analysis of the Mg AZ31B-SiC surface composite (Figure 16) reveals significant variations in grain refinement and reinforcement particle distribution based on the process parameters. The results indicate that specimen S2 (545 RPM, 31.5 mm/min, 0.58 mm groove width, Square Tool – SQ) exhibits the most uniform grain refinement and even distribution of SiC particles. The fine equiaxed grains observed in S2 are attributed to optimal dynamic recrystallization and controlled heat generation during friction stir processing (FSP). In contrast, specimens with excessive groove width (S3, S6, S7) show larger grain structures with irregular grain boundaries, which is caused by inadequate heat input and insufficient particle dispersion.

In lower feed rate specimens (S1, S4, S7), grain refinement is moderate, but grain size remains relatively large, indicating partial recrystallization due to prolonged heat exposure. However, at higher traverse speeds (S6, S9), finer grain structures were observed, but with uneven grain boundaries, suggesting that the reduced heat input. Additionally, higher rotational speeds (S7, S8, S9) resulted in excessive grain growth due to increased heat input, leading to coarsening rather than refinement. The most balanced grain refinement and particle dispersion are observed in S2, where moderate rotational and traverse speeds ensure optimal plastic deformation and uniform particle reinforcement.

Scanning electron microscopy (SEM) to analyze grain refinement and reinforcement particle distribution

The SEM images (Figure 17) provide a detailed analysis of the SiC particle distribution and interfacial bonding across the processed zone. Specimen S2 demonstrates the most homogeneous particle distribution, with minimal clustering and voids, ensuring effective load transfer and improved mechanical properties. The uniform dispersion of SiC particles in S2 suggests that the moderate groove width (0.58 mm) allowed for even particle incorporation without excessive agglomeration or segregation.

Conversely, specimens with larger groove widths (S3, S6, S7) show severe particle clustering and localized agglomeration, leading to weak zones and reduced strength. This clustering is evident in S3, where SiC particles are concentrated in isolated pockets rather than being uniformly distributed, contributing to lower mechanical properties. In S7 and S8 (high rotational speed specimens), excessive heat generation causes particle coarsening and partial dissolution, affecting the reinforcement's effectiveness.

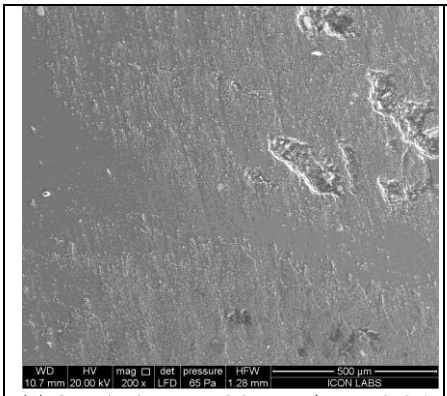

(a) S1: 545 RPM, 20 mm/min, 0.26 mm groove width, Tapered Threaded Tool (TT)

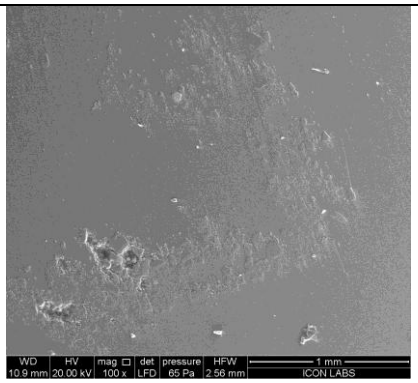

(b) S2: 545 RPM, 31.5 mm/min, 0.58 mm groove width, Square Tool (SQ)

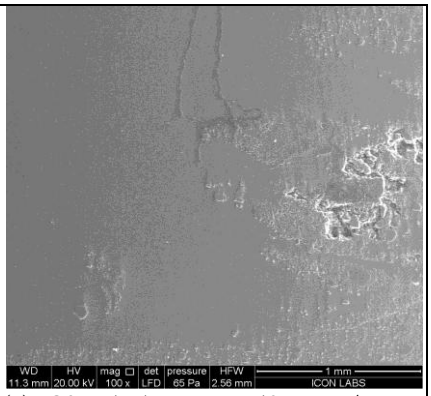

(c) S3: 545 RPM, 50 mm/min, 1.032 mm groove width, Cylindrical Threaded Tool (Cy TH)

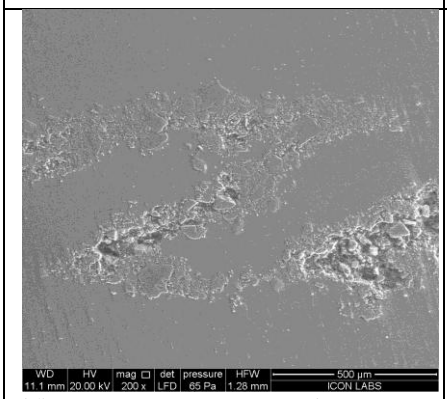

(d) S4: 765 RPM, 20 mm/min, 0.58 mm groove width, Cylindrical Threaded Tool (Cy TH)

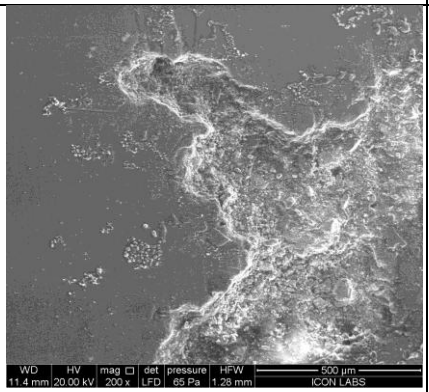

(e) S5: 765 RPM, 31.5 mm/min, 1.032 mm groove width, Tapered Threaded Tool (TT)

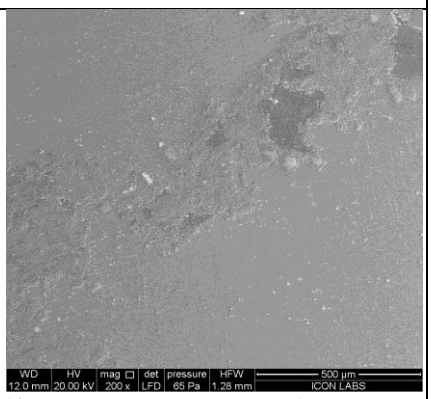

(f) S6: 765 RPM, 50 mm/min, 0.26 mm groove width, Square Tool (SQ)

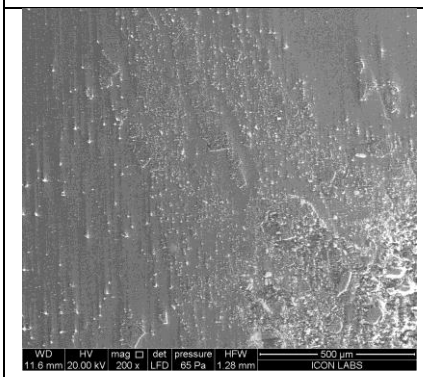

(g) S7: 1070 RPM, 20 mm/min, 1.032 mm groove width, Square Tool (SQ)

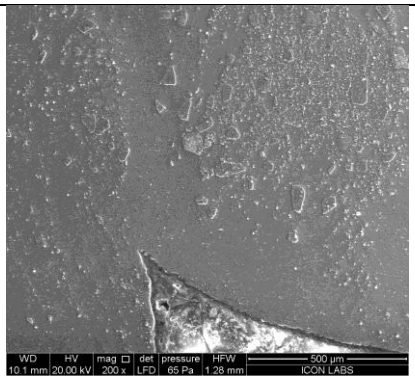

(h) S8: 1070 RPM, 31.5 mm/min, 0.26 mm groove width, Cylindrical Threaded Tool (TH)

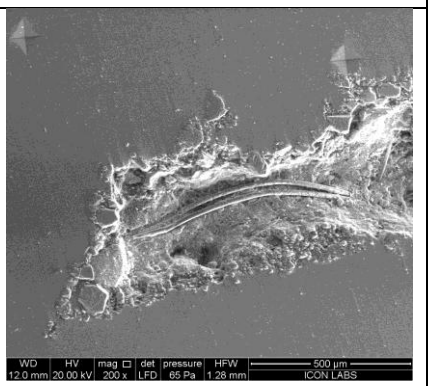

(i) S9: 1070 RPM, 50 mm/min, 0.58 mm groove width, Tapered Threaded Tool (TT)

Figure 17 (a-i) SEM for Specimen S1 to S9

Additionally, S1, S4, and S9 show regions of poor bonding and void formation, which can be attributed to insufficient material flow and ineffective stirring action. These defects reduce the interfacial strength between the matrix and reinforcement, leading to decreased mechanical performance. The optimal combination of uniform particle dispersion, strong interfacial bonding, and minimal defects is observed in S2, confirming that moderate process parameters (545 RPM, 31.5 mm/min, 0.58 mm groove width) provide the best reinforcement distribution and bonding characteristics.

CONCLUSION

The study found that groove width and pin profile significantly impacted the mechanical properties of Mg alloy reinforced with SiC. A groove width of 0.58 mm provided the optimal combination of ultimate tensile strength, percentage of elongation, and hardness. The square-headed pin profile yielded the highest mechanical properties,

making it the most effective tool design for reinforcement distribution. These findings offer insights for optimizing friction stir processing parameters to achieve superior material properties. The 0.58 mm groove width and the square-headed pin profile were the optimal process parameters for enhanced strength, and ductility in friction stir processing of Mg Alloy reinforced with SiC. The analysis indicates that a rotational speed of 545 RPM generates the highest ultimate tensile strength and hardness values. Additionally, a feed rate of 31.5 mm/min provides a 23.3% improvement in ultimate tensile strength. Furthermore, a groove width of 0.58 mm results in an 8.2% increase in ultimate tensile strength. Lastly, the findings demonstrate that the Square Headed tool pin profile exhibits the highest ultimate tensile strength and hardness measurements.

This study successfully fabricated and characterized AZ31B-SiC surface composites using Friction Stir Processing with the groove method. The key conclusions drawn from the research are:

Optimal Process Parameters: The combination of a square tool geometry, 545 rpm rotational speed, 31.5 mm/min traverse speed, and 0.58 mm groove width resulted in the best mechanical performance, demonstrating superior tensile strength, hardness, and uniform reinforcement dispersion.

Effect of Tool Geometry: The square tool profile exhibited the most effective material mixing, leading to minimal porosity and improved grain refinement, while the tapered threaded tool showed the highest reinforcement clustering.

Impact of Traverse Speed and Groove Width: Lower traverse speeds facilitated better reinforcement dispersion, whereas excessive speeds caused material softening and microstructural defects. Similarly, moderate groove widths (0.58 mm) ensured optimal mechanical properties, whereas wider grooves led to reinforcement clustering.

Microstructural Improvement: SEM and Optical Microscopy confirmed enhanced grain refinement and uniform SiC dispersion under optimized conditions, validating the effectiveness of the groove method in FSP.

Acknowledgement: The authors would like to express sincere gratitude to Mechanical Department Research centre, Savitribai Phule Pune University, Pune.

Data availability statement: All data that support the findings of this study are included within the article (and any supplementary files).

REFERENCES

[1] Boopathi Sampath and V. Haribalaji, "Influences of Welding Parameters on Friction Stir Welding of Aluminum and Magnesium: A Review," in *Materials Research Proceedings 19*, Oct. 2021, pp. 222–230. doi: 10.21741/9781644901618-28.

[2] K. Tesař, H. Somekawa, and A. Singh, "Development of texture and grain size during extrusion of ZA63 alloy containing stable quasicrystalline i-phase and its effect on tensile and compression strength," *J Alloys Compd*, vol. 849, p. 156340, Dec. 2020, doi: 10.1016/j.jallcom.2020.156340.

[3] "Zheng Tingjian, Zhang Lixia, and Liao Juan. 'Ultrasonic Vibration-Assisted Tensile Mechanical Behavior of Magnesium Alloy Plate and Constitutive Mold.' Chinese Journal of Plasticity Engineering 27, No. 12 (2020): 170-176.".

[4] J. Tan and S. Ramakrishna, "Applications of Magnesium and Its Alloys: A Review," *Applied Sciences*, vol. 11, no. 15, p. 6861, Jul. 2021, doi: 10.3390/app11156861.

[5] J. Chen, L. Tan, X. Yu, I. P. Etim, M. Ibrahim, and K. Yang, "Mechanical properties of magnesium alloys for medical application: A review," *J Mech Behav Biomed Mater*, vol. 87, pp. 68–79, Nov. 2018, doi: 10.1016/j.jmbbm.2018.07.022.

[6] V. K. Parikh, A. D. Badgujar, and N. D. Ghetiya, "Joining of metal matrix composites using friction stir welding: a review," *Materials and Manufacturing Processes*, vol. 34, no. 2, pp. 123–146, Jan. 2019, doi: 10.1080/10426914.2018.1532094.

[7] P. Vijayakumar, K. Pazhanivel, N. Ramadoss, A. Ganeshkumar, K. Muruganantham, and M. Arivanandhan, "Synthesis and Characterization of AZ91D/SiC/BN Hybrid Magnesium Metal Matrix Composites," *Silicon*, vol. 14, no. 16, pp. 10861–10871, Nov. 2022, doi: 10.1007/s12633-022-01823-3.

[8] K. S. A. Ali *et al.*, "Mechanical and Microstructural Characterization of Friction Stir Welded SiC and B4C Reinforced Aluminium Alloy AA6061 Metal Matrix Composites," *Materials*, vol. 14, no. 11, p. 3110, Jun. 2021, doi: 10.3390/ma14113110.

[9] P. Samal, P. R. Vundavilli, A. Meher, and M. M. Mahapatra, "Recent progress in aluminum metal matrix composites: A review on processing, mechanical and wear properties," *J Manuf Process*, vol. 59, pp. 131–152, Nov. 2020, doi: 10.1016/j.jmapro.2020.09.010.

[10] C. Zhang, Z. Li, J. Zhang, H. Tang, and H. Wang, "Additive manufacturing of magnesium matrix composites: Comprehensive review of recent progress and research perspectives," *Journal of Magnesium and Alloys*, vol. 11, no. 2, pp. 425–461, Feb. 2023, doi: 10.1016/j.jma.2023.02.005.

[11] S. Jhamb, J. Matai, J. Marwaha, A. Goyal, and A. Pandey, "A comprehensive analysis on magnesium-based alloys and metal matrix composites for their in-vitro biocompatibility," *Advances in Materials and Processing Technologies*, vol. 9, no. 3, pp. 1249–1282, Jul. 2023, doi: 10.1080/2374068X.2022.2113521.

[12] J. Long *et al.*, "Effects of minor Zr addition on the microstructure and mechanical properties of laser welded joint of Al/SiCp metal-matrix composite," *J Manuf Process*, vol. 49, pp. 373–384, Jan. 2020, doi: 10.1016/j.jmapro.2019.12.004.

[13] S. K. Selvaraj *et al.*, "Contemporary Progresses in Ultrasonic Welding of Aluminum Metal Matrix Composites," *Front Mater*, vol. 8, Apr. 2021, doi: 10.3389/fmats.2021.647112.

[14] L. Ma, C. Zhou, Q. Wen, M. Li, H. Zhong, and S. Ji, "Ultrasonic-promoted rapid transient liquid phase bonding of high volume fraction SiC particle reinforced aluminum-based metal matrix composite in low temperature," *Ultrasonics*, vol. 106, p. 106159, Aug. 2020, doi: 10.1016/j.ultras.2020.106159.

[15] C. Wang *et al.*, "Effect of tool offsetting on friction stir welding of dissimilar aluminium matrix composite and aluminium alloy," *Science and Technology of Welding and Joining*, vol. 27, no. 7, pp. 586–593, Oct. 2022, doi: 10.1080/13621718.2022.2091342.
[16] *Mishra SC. Analysis of experimental results of plasma spray coatings using statistical techniques. BOOK: Advanced Plasma Spray Applications, Published by InTech, Printed in Croatia. 2012 Mar 21:83-96.*
[17] K. Palanikumar, E. Natarajan, S. Suresh, D. G. Mohan, C. Prakash, and K. Kaur, "Prospects of friction stir processed Mg alloys and composites-Reviews and suggestions," *Journal of Materials Research and Technology*, vol. 31, pp. 971–997, Jul. 2024, doi: 10.1016/j.jmrt.2024.06.087.
[18] J. A. del Valle, P. Rey, D. Gesto, D. Verdera, J. A. Jiménez, and O. A. Ruano, "Mechanical properties of ultra-fine grained AZ91 magnesium alloy processed by friction stir processing," *Materials Science and Engineering: A*, vol. 628, pp. 198–206, Mar. 2015, doi: 10.1016/j.msea.2015.01.030.
[19] Q. Zang, H. Chen, F. Lan, J. Zhang, and Y. Jin, "Effect of friction stir processing on microstructure and damping capacity of AZ31 alloy," *J Cent South Univ*, vol. 24, no. 5, pp. 1034–1039, May 2017, doi: 10.1007/s11771-017-3506-9.
[20] A. Raja, P. Biswas, and V. Pancholi, "Effect of layered microstructure on the superplasticity of friction stir processed AZ91 magnesium alloy," *Materials Science and Engineering: A*, vol. 725, pp. 492–502, May 2018, doi: 10.1016/j.msea.2018.04.028.
[21] F. K. MD and S. K. Panigrahi, "Achieving excellent superplasticity in an ultrafine-grained QE22 alloy at both high strain rate and low-temperature regimes," *J Alloys Compd*, vol. 747, pp. 71–82, May 2018, doi: 10.1016/j.jallcom.2018.02.294.
[22] H. Singh Sidhu, B. Singh, and P. Kumar, "To study the corrosion behavior of friction stir processed magnesium alloy AZ91," *Mater Today Proc*, vol. 44, pp. 4633–4639, 2021, doi: 10.1016/j.matpr.2020.10.920.
[23] Q. Shang, D. R. Ni, P. Xue, B. L. Xiao, K. S. Wang, and Z. Y. Ma, "An approach to enhancement of Mg alloy joint performance by additional pass of friction stir processing," *J Mater Process Technol*, vol. 264, pp. 336–345, Feb. 2019, doi: 10.1016/j.jmatprotec.2018.09.021.
[24] V. Patel *et al.*, "Tailoring grain refinement through thickness in magnesium alloy via stationary shoulder friction stir processing and copper backing plate," *Materials Science and Engineering: A*, vol. 784, p. 139322, May 2020, doi: 10.1016/j.msea.2020.139322.
[25] A. A. Luo, "Magnesium casting technology for structural applications," *Journal of Magnesium and Alloys*, vol. 1, no. 1, pp. 2–22, Mar. 2013, doi: 10.1016/j.jma.2013.02.002.
[26] C. R. F. Azevedo, E. Hippert, G. Spera, and P. Gerardi, "Aircraft landing gear failure: fracture of the outer cylinder lug," *Eng Fail Anal*, vol. 9, no. 1, pp. 1–15, Feb. 2002, doi: 10.1016/S1350-6307(00)00039-X.
[27] "535.0, A535.0, and B535.0," in *Properties and Selection of Aluminum Alloys*, ASM International, 2019, pp. 583–584. doi: 10.31399/asm.hb.v02b.a0006585.
[28] B. R. Powell, P. E. Krajewski, and A. A. Luo, "Magnesium alloys for lightweight powertrains and automotive structures," in *Materials, Design and Manufacturing for Lightweight Vehicles*, Elsevier, 2021, pp. 125–186. doi: 10.1016/B978-0-12-818712-8.00004-5.
[29] G. Zhang, S. Qin, L. Yan, and X. Zhang, "Simultaneous improvement of electromagnetic shielding effectiveness and corrosion resistance in magnesium alloys by electropulsing," *Mater Charact*, vol. 174, p. 111042, Apr. 2021, doi: 10.1016/j.matchar.2021.111042.
[30] M. Rahman, Y. Li, and C. Wen, "HA coating on Mg alloys for biomedical applications: A review," *Journal of Magnesium and Alloys*, vol. 8, no. 3, pp. 929–943, Sep. 2020, doi: 10.1016/j.jma.2020.05.003.
[31] Y. Yang, X. Xiong, J. Chen, X. Peng, D. Chen, and F. Pan, "Research advances of magnesium and magnesium alloys worldwide in 2022," *Journal of Magnesium and Alloys*, vol. 11, no. 8, pp. 2611–2654, Aug. 2023, doi: 10.1016/j.jma.2023.07.011.
[32] C. Vidal *et al.*, "Particles' distribution enhancing in aluminum-based composites produced by upward friction stir processing," *The International Journal of Advanced Manufacturing Technology*, vol. 127, no. 5–6, pp. 2745–2757, Jul. 2023, doi: 10.1007/s00170-023-11664-y.
[33] A. Thangarasu, S. Boovendra Varma, and S. Sudharsan, "Microstructure and wear behaviour of aluminium surface composites fabricated using friction stir processing," *IOP Conf Ser Mater Sci Eng*, vol. 932, no. 1, p. 012132, Sep. 2020, doi: 10.1088/1757-899X/932/1/012132.
[34] Y. Gao *et al.*, "CNTs distribution and ductility improvement mechanisms in oscillating laser-arc hybrid welding of AZ31B magnesium alloy," *Compos Part A Appl Sci Manuf*, vol. 164, p. 107280, Jan. 2023, doi: 10.1016/j.compositesa.2022.107280.
[35] S. Singla, A. S. Kang, P. Sagar, and A. Handa, "Recent Advances in Magnesium-Based Metal Matrix Surface Composites Developed via Friction Stir Processing Route—An Overview," *Metallography, Microstructure, and Analysis*, vol. 12, no. 6, pp. 1068–1068, Dec. 2023, doi: 10.1007/s13632-023-01030-5.
[36] "Test Methods for Tension Testing of Metallic Materials," May 01, 2022, *ASTM International, West Conshohocken, PA*. doi: 10.1520/E0008_E0008M-22.
[37] "Test Methods for Vickers Hardness and Knoop Hardness of Metallic Materials," Apr. 01, 2017, *ASTM International, West Conshohocken, PA*. doi: 10.1520/E0092-17.